Journal of Alloys and Compounds 506 (2010) 120–124

Contents lists available at ScienceDirect

Journal of Alloys and Compounds

journal homepage: www.elsevier.com/locate/jallcom

Phase evolution and PEC performance of $Zn_xCd_{(1-x)}S$ nanocrystalline thin films deposited by CBD

P.B. Bagdare, S.B. Patil, A.K. Singh*

Defence Institute of Advanced Technology (DU), Girinagar, Pune 411025, Maharashtra, India

ARTICLE INFO

Article history:
Received 7 April 2010
Received in revised form 17 June 2010
Accepted 24 June 2010
Available online 3 July 2010

Keywords:
CBD
Nanocrystalline
Morphology
EIS
PEC

ABSTRACT

Thin films of $Zn_xCd_{(1-x)}S$ with varying Zn concentration, $0.1 \leq x \leq 0.9$, were successfully deposited on stainless steel (SS) and amorphous glass substrate by simple and convenient chemical bath deposition (CBD) technique. Prepared films were annealed at 523 K for 1 h and used for structural, optical and morphological characterization. XRD studies confirm the nanocrystalline nature with cubic and hexagonal phases of CdS and ZnS, and diffraction peak intensity decreased with increase in x. The blue shift in the optical transmission spectra was found with increase in x. An interesting change in morphology, from flake to spherical particle structure, was observed with increase in Zn concentration. Electrochemical Impedance Spectroscopy (EIS) was carried out for all the films. These films were successfully utilized for photoelectrochemical (PEC) cell application. The charge transfer resistance (R_{ct}) determined from nyquist plots were found to be decreased initially with increase in x, minimum for $x = 0.5$ and increased thereafter. The performance of PEC cell was found to be dependent on the concentration of Zn and efficiency was found to be increased with increasing x, maximum for $x = 0.5$ and decreased thereafter. The maximum short circuit current density (J_{sc}) and open circuit voltage (V_{oc}) i.e. 457 μA/cm^2 and 389 mV were respectively found for $x = 0.5$ under 10 mW/cm^2 of illumination.

1. Introduction

After Honda–Fujishima effect a variety of PEC solar cells have been fabricated and investigated. Thin film based PEC solar cells [1–3] have wide applications due to their low fabrication cost, high throughput processing techniques and ease of junction formation with an electrolyte. The semiconductors with bandgap close to the maximum wavelength in the visible spectrum are promising materials for the PEC cells. CdS, belonging to II–VI groups, is one of the promising semiconductors, having bulk bandgap 2.42 eV. It also acts as window layer in CdTe [4] and copper indium (di) selenide [5] as well as copper indium gallium (di) selenide [6] based solar cells. But the disadvantage of CdS is that it degrades into soluble cadmium cations under PEC conditions which are hazardous [7]. This would limit the use of CdS as a photoelectrode material for PEC cell unless its characteristics are modified. To overcome this problem doping of CdS by Zn has been explored.

There are various techniques to produce thin films of $Zn_xCd_{(1-x)}S$ like chemical vapor deposition [8] electrochemical deposition [9], successive ionic layer adsorption and reaction technique [10] and CBD [11,12]. However, CBD method appears suitable for large area industrial process. It is the least expensive and a low temperature method that makes it very attractive. Another advantage of the CBD technique is its ability to deposit very thin films (50 nm) in a conformal manner on a rough substrate surface. Thin films of pure CdS by CBD with different capping agents have been deposited by Patil and Singh [13] for PEC cell application. Hankare et al. [14,15] have deposited the thin films of pure ZnS by dip method and have studied the PEC properties. Innocenti et al. [16] have deposited thin films of $Cd_xZn_{(1-x)}S$ ($x = 0.3$) on Ag(1 1 1) substrate by electrochemical atomic layer epitaxy (ECALE) and utilized for PEC cell application. Superlattice of ZnS/CdS on Au(1 1 1), deposited by ECALE, has been used for PEC cell application by Torimoto et al. [17]. Thin films of $Zn_xCd_{(1-x)}S$ have been utilized as a window material in photovoltaic cells [18].

To the best of our knowledge there is no report on chemically bath deposited $Zn_xCd_{(1-x)}S$ thin films for PEC cell application. In this report we present, bath deposition of $Zn_xCd_{(1-x)}S$ thin films (from aqueous solutions) on glass as well as SS substrate by CBD. The phase evolution and enhancement in the PEC performance has been discussed as the performance of cell depends on grain morphology, interface properties and doping level.

2. Experimental

A simple CBD method was employed to deposit $Zn_xCd_{(1-x)}S$ ($0.1 \leq x \leq 0.9$) thin films on to SS and amorphous glass substrates using thiourea as sulfide ion source,

* Corresponding author. Tel.: +91 2024304173; fax: +91 2024389411.
E-mail addresses: draksingh@hotmail.com, aksingh@diat.ac.in (A.K. Singh).

0925-8388/$ – see front matter © 2010 Elsevier B.V. All rights reserved.
doi:10.1016/j.jallcom.2010.06.152

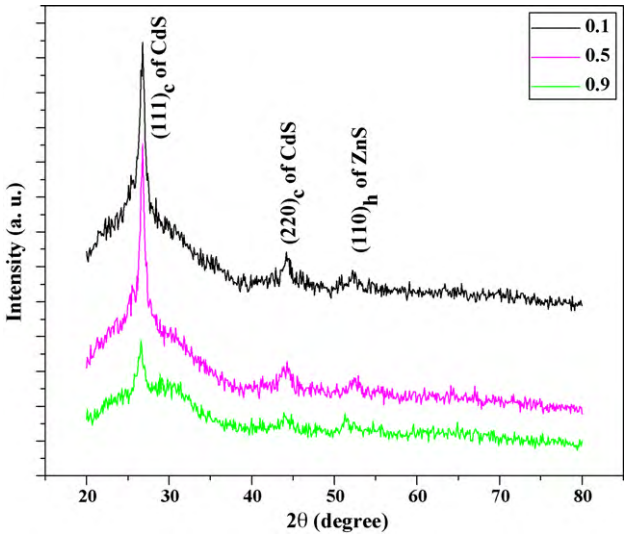

Fig. 1. XRD pattern of $Zn_xCd_{(1-x)}S$ thin films for selected values of x (0.1, 0.5, and 0.9).

$CdSO_4$ and $ZnSO_4$ as a cadmium and zinc ion source respectively. Triethanolamine was used as a complexing agent and to maintain the pH liquid ammonia was used. All the solutions were aqueous based prepared using de-ionized (DI) water having resistivity 18.2 MΩ. Synthesis details are discussed by Chavhan and Sharma [11] for the deposition of Zn_{1-x} Cd_xS thin films of different Zn compositions. After deposition, the samples were removed from bath and washed with DI water until heterogeneities are removed. Prepared films were air annealed at 523 K for 1 h. Before use the substrates were cleaned with laboline detergent, thoroughly washed with DI water and boiled in dilute chromic acid. Finally these substrates were sonicated in water bath for 15 min. The films on amorphous glass substrate were used for structural, optical and morphological studies and the films on SS substrate were utilized for EIS and PEC cell studies.

Crystallographic study was carried out using Bruker AXS, Germany (Model D8 Advanced) diffractometer in the scanning range of 20–80° (2θ) using Cu Ka radiations of wavelength 1.5045 Å. JEOL ASM 6360A scanning electron microscope (SEM) was used to study the morphology of the films and the elemental analysis. Room temperature optical transmission spectra of samples were recorded in the wavelength range of 350–750 nm using Ocean Optics HR4000 high-resolution spectrometer. EIS and PEC properties were studied using VersaSTAT3 Potentiostat/Galvanostat, Princiton Applied Research. Three-electrode system was used for EIS studies in which films on SS substrate were used as a working electrode, platinum mesh as a counter electrode and saturated calomel electrode (SCE) as a reference electrode. Films were placed in the Teflon holder with a Teflon washer having 10 mm internal diameter determining the exposed area. Sulfide/polysulfide of composition NaOH (0.1 M), S (0.1 M) and Na_2S (0.1 M) was used as electrolyte. The frequency range examined was 1 MHz to 100 mHz. The PEC cell was fabricated with three-electrode system in which CdS films on SS substrate was used as a working electrode (active photoelectrode), graphite as counter electrode and SCE as a reference electrode. Sulfide/polysulfide electrolyte of same composition was used as redox couple. A tungsten filament lamp of 230 V/50 W was used as a source of white light to illuminate the PEC cell. The measured illumination intensity was 10 mW/cm^2 at the interface.

3. Results and discussions

3.1. Crystallographic studies

The X-ray diffractograms of $Zn_xCd_{1-x}S$ film for selected x values are shown in Fig. 1.

The observed initial broad hump is due to amorphous glass substrate. The diffraction pattern shows that films crystallized in both the cubic and hexagonal phases with prominent diffraction lines of CdS [(1 1 1)c and (2 2 0)c] and ZnS [(1 1 0)h]. The intensities of diffracted peaks that arose from cubic phase of CdS were found to be decreased with the increasing value of x. It can be attributed to the increased amorphous phase of ZnS. The diffraction peaks appear enlarged due to smaller grain size.

Table 1
Comparison of various parameters of $Zn_xCd_{(1-x)}S$ thin films with change in x.

x	Crystallite, size (nm)	R_{ct} (Ω)	J_{sc} (μA/cm^2)	V_{oc} (mV)	Efficiency, η (%)
0.1	26	9.5	37	57	0.007
0.2	–	9	139	238	0.106
0.3	–	8.5	215	254	0.159
0.4	–	8	348	309	0.353
0.5	19	7	457	389	0.673
0.6	–	9.5	87	140	0.045
0.7	–	10	78	100	0.025
0.8	–	10.5	48	71	0.011
0.9	8	11.5	26	46	0.004

Assuming a homogeneous strain across the crystallites, the size of the crystallites can be estimated using the Scherrer's formula.

$$D = \frac{k\lambda}{\beta \cos\ \theta} \quad (1)$$

where 'λ' is the wavelength of X-rays and 'θ' the Bragg's angle (in radian), k is a constant, β is the full width at half-maximum (FWHM). The calculated average crystallite sizes are in the range of 8–26 nm, shown in the Table 1, which confirm the nanocrystalline nature of the films.

In order to study the chemical composition of the thin films, EDAX measurements were performed on the samples. Fig. 2 shows a typical EDAX spectrum for the selective values of x. In addition to peaks for Cd, Zn and S peak corresponding to silicon, which arose from the glass substrates, were observed for all the samples. Increased in peak count for Zn in expense of Cd was observed.

3.2. Optical studies

Fig. 3 shows the room temperature optical transmission spectra of the films recorded in the range of 350–750 nm. The absorption edge for $x = 0.1$ is observed at around 525 nm (close to CdS room temperature energy gap 2.4–2.5 eV), which corresponds with the clear yellow-orange color of the samples. On increasing the x values slight blue shift in absorption edge has been observed. Similar results have been reported by Borse et al. [19]. It can be attributed to decrease in the crystallite size with increase in x, which is confirmed from XRD pattern.

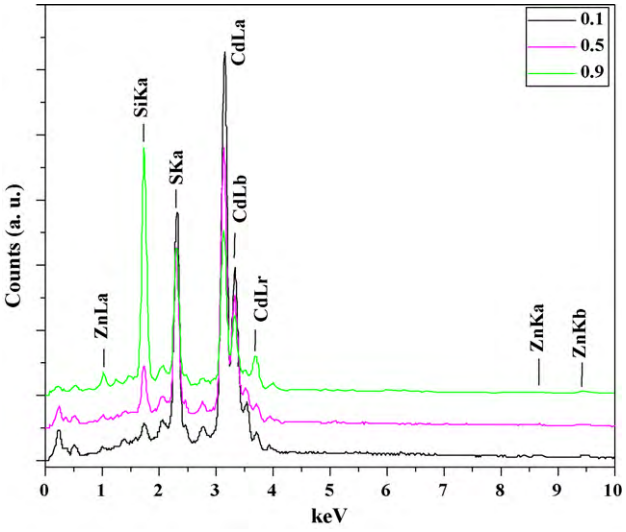

Fig. 2. EDAX spectra of $Zn_xCd_{(1-x)}S$ thin films for selected values of x (0.1, 0.5, and 0.9).

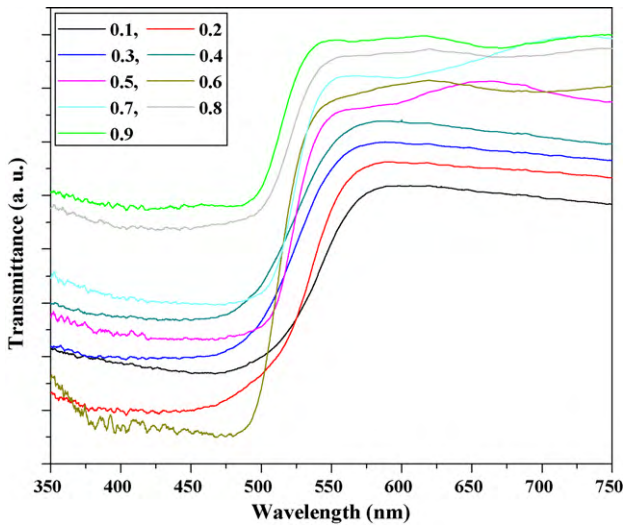

Fig. 3. Room temperature optical transmission spectra of $Zn_xCd_{(1-x)}S$ thin films for all x (0.1–0.9).

3.3. Morphological studies

The SEM micrographs of $Zn_xCd_{1-x}S$ film for selected x values (0.1, 0.2, 0.4, 0.5, 0.6 and 0.9) are shown in Fig. 4. For lower values of x (0.1–0.4) the flake like morphology has been observed (Fig. 4a–c). Similar morphology has been reported by Patil et al. [13] for CdS thin films grown by CBD. Chavhan et al. [12] have reported nanosheet morphology of $Zn_xCd_{(1-x)}S$ ($x = 0.1$) thin films deposited by CBD method. An interesting change in morphology has been observed with increasing Zn concentration. The flake like morphology gradually converted into spherical particle like morphology (Fig. 4c–f). The change in morphology may be due to difference in ionic radii and also formation of separate ZnS phase as can be seen from XRD pattern. The mean size of individual agglomerated grains is around 200–300 nm.

3.4. EIS studies

To investigate the properties of the interface formed between the $Zn_xCd_{1-x}S$ photoelectrode and sulfide/polysulfide electrolyte EIS studies have been carried out in dark at open cell voltage. Fig. 5a

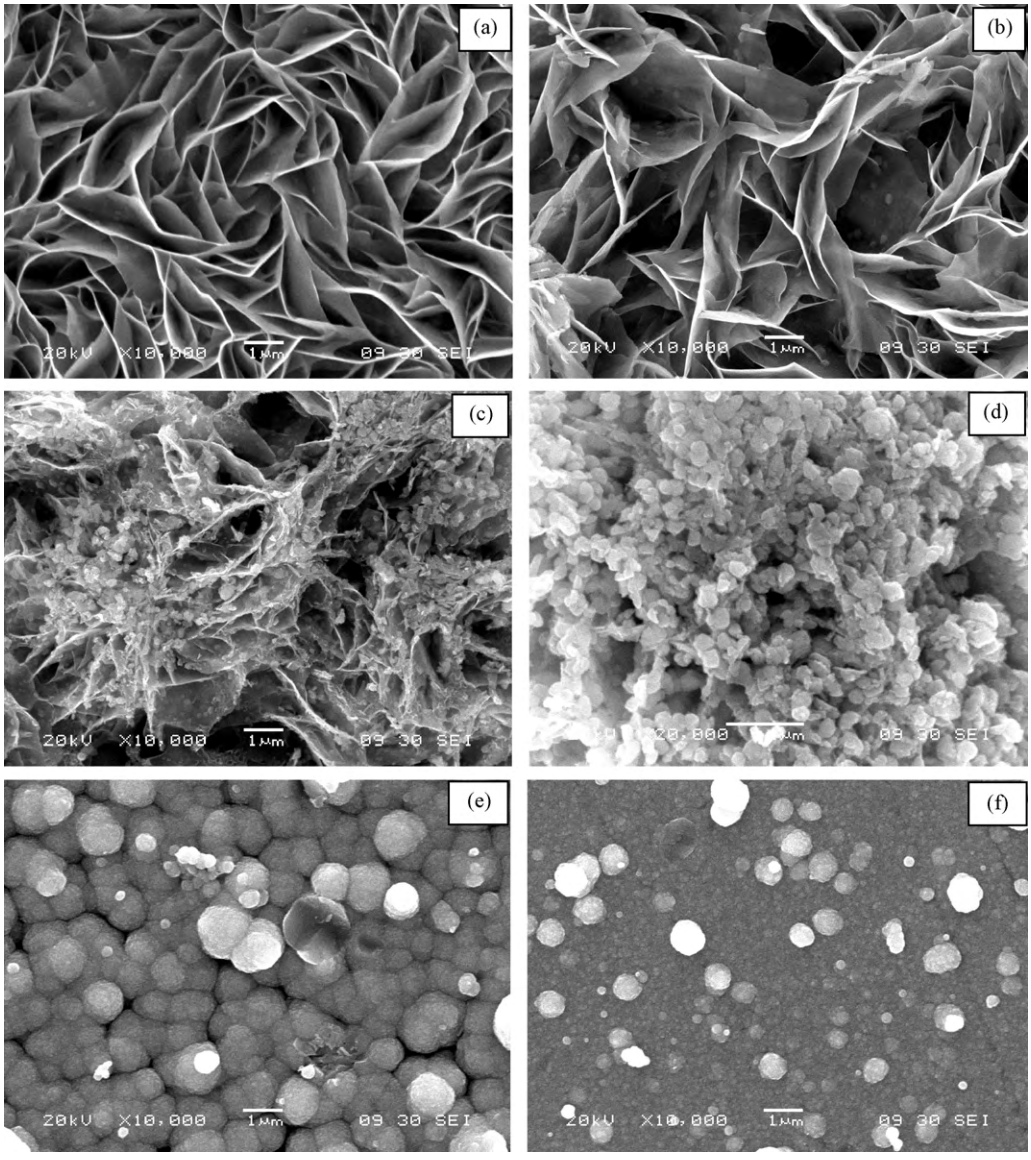

Fig. 4. SEM micrographs of the $Zn_xCd_{(1-x)}S$ thin films for selected values of x (a) 0.1, (b) 0.2, (c) 0.4, (d) 0.5, (e) 0.6, and (f) 0.9.

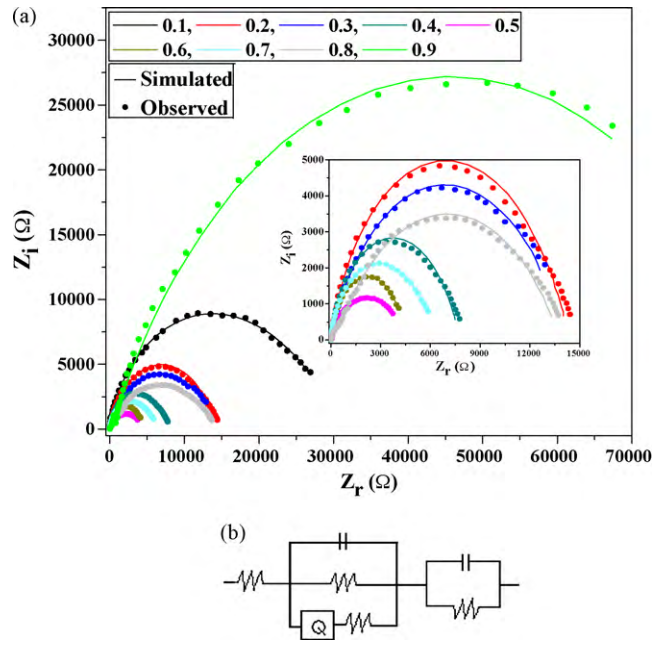

Fig. 5. (a) Nyquist plots for all x (0.1–0.9) recorded at open circuit volatge with frequency range 1 MHz to 100 mHz. Inset of the figure shows the expanded region of nyquist plots for x (0.2–0.8). (b) Equivalent circuit for the observed nature of the nyquist plots.

shows the Nyquist plots of all samples. The inset of the figure shows the enlarged view of Nyquist plots for $0.2 \leq x \leq 0.8$. The experimental data have been compared with different equivalent circuits with the ZSimpWin 3.21 EChem Software and the best fit is shown in the Fig. 5b. The presence of the term Q (leaking capacitor) may be due to diffusion of Cd^{2+} ions across the double layer capacitance to the electrolyte [13]. Value of the R_{ct} was taken to be the half of the real component of impedance which appeared as semicircle at the high frequency end of the EIS spectrum [20] and reported in the Table 1. The R_{ct} between the electrode and the electrolyte appears as a voltage loss at the counter electrode and it contributes directly to the series resistance of the whole cell [21]. The series resistance mainly attributed to the resistance of the conducting substrate, electrolyte and counter electrode/electrolyte interface. Initially the R_{ct} values have been found to be decreased with increasing value of x, it is minimum for $x = 0.5$ and thereafter increased with increasing value of x. These values of R_{ct} are important to limit the values of J_{sc} and V_{oc}.

3.5. PEC properties

When a photoelectrode is immersed in an electrolyte an electrode–electrolyte interface is formed which is called PEC cell. As soon as photoelectrode is immersed in an electrolyte charge transfer takes place across the interface, which in turns forms depletion region across the interface. This depletion region is driving force for the current–voltage characteristics in dark and under illumination. Fig. 6 shows the J–V characteristics under 10 mW/cm^2 of illumination. As the photovoltage behavior is cathodic, seen from the figure, all samples are of n-type. The values of J_{sc} and V_{oc}, for $x = 0.1$, are found to be 37 μA/cm^2 and 57 mV respectively. Both the values of J_{sc} and V_{oc} have been found to be increased with increasing x initially, as can be seen from the Fig. 6, maximum for $x = 0.5$ and decreased rapidly thenceforth. The increased values of J_{sc} and V_{oc} in turn increased the conversion efficiency of the cell. Fig. 7 shows the behavior of J_{sc} and V_{oc} with x. The variations, which increased initially and decreased thereafter, in J_{sc} and V_{oc} can be attributed

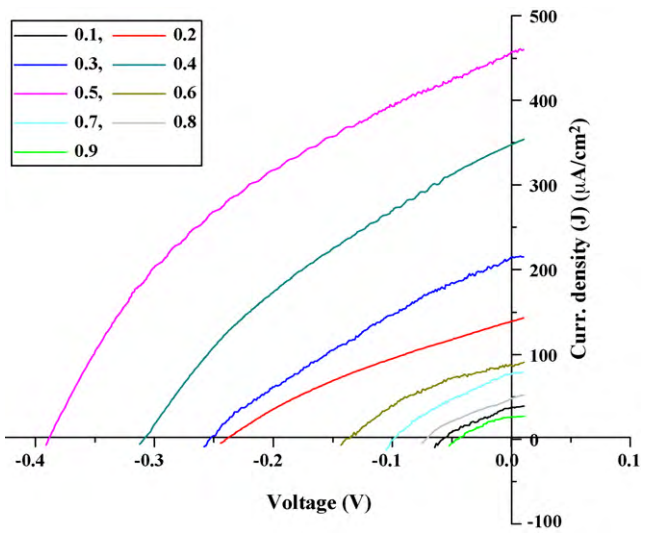

Fig. 6. Photo J–V plots for all x (0.1–0.9) under 10 mW/cm^2 of illumination.

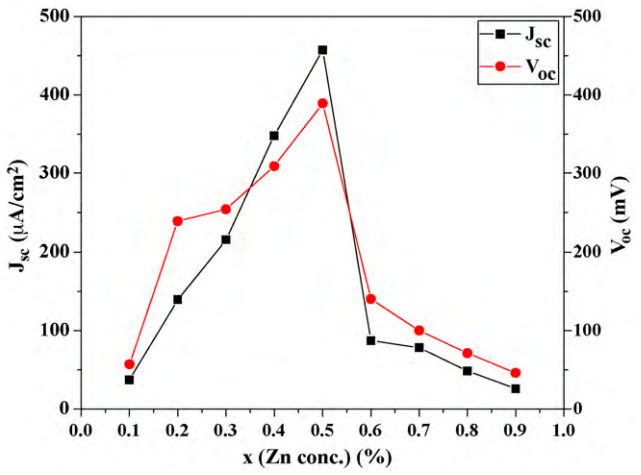

Fig. 7. The behavior of J_{sc} and V_{oc} with x.

to the variation in R_{ct} values with increasing x. This behavior can be explained on the basis of crystallite size, phase evolution and R_{ct}. The PEC performance of these films is initially controlled by crystallite size i.e. performance is increased with decreasing crystallite size and increasing phase of ZnS, it increased up to $x = 0.5$, and then by resistance since the resistance of the films increases with decreasing size of crystallite. The values of J_{sc} and V_{oc} were found to be maximum, 457 μA/cm^2 and 389 mV respectively, for $x = 0.5$ and hence the maximum efficiency. The PEC cell performance obtained for $x = 0.5$ is better than the PEC cell performance reported by Patil et al. [13] for CdS thin films.

The values of J_{sc}, V_{oc}, and efficiency (η) are reported in Table 1.

4. Conclusion

The nanocrystalline thin films of $Zn_xCd_{(1-x)}S$ with $0.1 \leq x \leq 0.9$ were deposited successfully on steel substrate by simple and convenient chemical bath deposition technique. Morphology change, from flake like to spherical particle like, and phase evolution were observed with increasing x. Both cubic and hexagonal phases of CdS and hexagonal phase of ZnS were identified in crystal studies. The slight blue shift in the optical absorption was observed with increasing x. The EIS results showed that R_{ct} initially decreased with increasing x, it was minimum for $x = 0.5$, and again increased

with further increase in x. The PEC performance was found to be increased initially with increasing x, it was maximum for $x = 0.5$, and decreased thenceforth with further increment in x. The observed J_{sc} and V_{oc} for $x = 0.5$ were 457 μA/cm^2 and 389 mV respectively under 10 mW/cm^2 of illumination. The composition $Zn_xCd_{(1-x)}S$ with $x = 0.5$ was found to be appropriate for PEC cell application.

Acknowledgements

Authors are thankful to Vice Chancellor, Defence Institute of Advanced Technology, Girinagar, Pune 411025 (India), for granting permission to publish this work. Authors are also thankful to University of Pune, Pune, for providing the SEM and XRD of the samples.

References

[1] J.K. Dongre, M. Ramrakhiani, J. Alloys Compd. 487 (2009) 653.
[2] W. Yao, S. Yu, S. Liu, J. Chen, X. Liu, F. Li, J. Phys. Chem. B 110 (2006) 11704.
[3] X. Ren, G. Zhao, H. Li, W. Wu, G. Han, J. Alloys Compd. 465 (2008) 534.
[4] J. Heo, H. Ahn, R. Lee, Y. Han, D. Kim, Solar Energy Mater. Solar Cells 75 (2003) 193.
[5] F. Kang, J. Ao, G. Sun, Q. He, Y. Sun, J. Alloys Compd. 478 (2009) L25.
[6] C.J. Hibberd, K. Ernits, M. Kaelin, U. Müller, A.N. Tiwari, Prog. Photovolt.: Res. Appl. 16 (2008) 585.
[7] A.H. Zyoud, N. Zaatar, I. Saadeddin, C. Ali, D. Park, G. Campet, H.S. Hilal, J. Hazard. Mater. 173 (2010) 318.
[8] M. Nyman, K. Jenkins, M.J.H. Smith, T.T. Kodas, E.N. Duester, A.L. Rheingold, M.L.L. Sands, Chem. Mater. 10 (1998) 914.
[9] F. Loglio, M. Innocenti, G. Pezzatini, M.L. Foresti, J. Electroanal. Chem. 562 (2004) 117.
[10] G. Laukaitis, S. Lindroos, S. Tamulevičius, M. Leskelä, M. Račkaitis, Appl. Surf. Sci. 161 (2000) 396.
[11] S. Chavhan, R.P. Sharma, J. Phys. Chem. Solids 66 (2005) 1721.
[12] S.D. Chavhan, S. Senthilarasu, S.H. Lee, Appl. Surf. Sci. 254 (2008) 4539.
[13] S.B. Patil, A.K. Singh, Appl. Surf. Sci. 256 (2010) 2884.
[14] P.P. Hankare, P.A. Chate, D.J. Sathe, J. Alloys Compd. 487 (2009) 367.
[15] P.P. Hankare, P.A. Chate, D.J. Sathe, B.V. Jadhav, J. Alloys Compd. 490 (2010) 350.
[16] M. Innocenti, S. Cattarin, F. Loglio, T. Cecconi, G. Seravalli, M.L. Foresti, Electrochim. Acta 49 (2004) 1327.
[17] T. Torimoto, A. Obayashi, S. Kuwabata, H. Yoneyama, Electrochem. Commun. 2 (2000) 359.
[18] F.A. Abouelfotouh, R.A. Awadi, M.M.A. Elnaby, Thin Solid Films 96 (1982) 169.
[19] S.V. Borse, S.D. Chavhan, R. Sharma, J. Alloys Compd. 436 (2007) 407.
[20] N. Papageorgiou, W.F. Maier, M. Grätzel, J. Electrochem. Soc. 144 (1997) 876.
[21] J. Halme, M. Toivola, A. Tolvanen, P. Lund, Solar Energy Mater. Solar Cells 90 (2006) 872.